Nonradial oscillations and gravitational wave emission of hybrid neutron stars

Zi-Yue Zheng (郑子岳), Ting-Ting Sun (孙婷婷), Huan Chen (陈欢),* and Jin-Biao Wei (魏金标)
School of Mathematics and Physics, China University of Geosciences, Lumo Road 388, 430074 Wuhan, China

G. F. Burgio and H.-J. Schulze
INFN Sezione di Catania, Dipartimento di Fisica, Universitá di Catania, Via Santa Sofia 64, 95123 Catania, Italy

(Received 10 March 2023; accepted 5 May 2023; published 25 May 2023)

We investigate nonradial oscillations of pure and hybrid neutron stars, employing equations of state of nuclear matter from Brueckner-Hartree-Fock theory, and of quark matter from the Dyson-Schwinger quark model, performing a Gibbs construction for the mixed phase in hybrid stars. Characteristic differences between neutron-star and hybrid-star g_1-mode oscillation frequencies, damping times, and gravitational wave strains are pointed out. Prospects of observations are also discussed.

DOI: 10.1103/PhysRevD.107.103048

I. INTRODUCTION

The interior of a neutron star (NS) can reach several times the nuclear saturation density $\rho_0 \simeq 0.16$ fm^{-3}. Therefore, there might exist a phase transition to deconfined quark matter (QM) in the NS core [1]. In general, once the equation of state (EOS) of nuclear matter (NM) is known, one can compute the structure and properties of NSs. Unfortunately, so far, due to the lack of exact computation dealing with the nonperturbative strong interaction, the EOS of high-density NM remains an open theoretical problem. There are many theoretical models for the NS EOS that can meet the observational and experimental constraints; see, e.g., [2] for a recent review. For NM in the hadron phase, popular EOSs are based on relativistic mean field models [3], phenomenological models based on energy-density functional theory with generalized Skyrme effective forces [4], Brueckner-Hartree-Fock (BHF) theory [5–9], the variational method [10], the self-consistent Green's function approach [11], and chiral effective field theory [12–15]. For QM, EOSs are mainly obtained with the MIT bag model [16], the Nambu-Jona-Lasinio model [17–19], the perturbative QCD [20–22], and the Dyson-Schwinger equations (DSEs) [23–27].

To test the various theoretical models of NSs and hybrid stars (HSs), we have to resort to observations. The mass-radius relation is one of the most straightforward and simple observables, which can be theoretically obtained by solving the Tolman-Oppenheimer-Volkov (TOV) equations combined with the EOS. Recently, several observed pulsars with masses above two solar masses [28–31] put firm lower limits on the maximum mass of NSs. Some theoretical analyses of the NS merger event GW170817 even deduce an upper limit on the maximum mass of about 2.2–2.3$M_\odot$ [32–36], albeit with large theoretical uncertainty. In 2019, new constraints on the radius were provided by the neutron star interior composition explorer (NICER) mission, which reported Bayesian parameter estimations of the mass and equatorial radius of the millisecond pulsar PSR J0030 + 0451 [37,38], and recently on PSR J0740 + 6620 with mass $2.08^{+0.07}_{-0.07} M_\odot$ [31,39–43].

However, it is hard to distinguish HSs and pure NSs from the mass-radius relations, since theoretically the differences between them are small, and even masked by the uncertainties of pure NSs with various models [44]. Therefore, one needs other observables to reveal the interior of NSs.

NSs are sources of electromagnetic waves in all wavelengths, and also emitters of both continuous and inspiral gravitational waves (GWs). In particular, when NSs experience violent processes such as accretions, radial and nonradial oscillations, glitches, and even NS mergers [45,46], they are expected to emit strong enough signals that can be observed. After the first direct observation of GWs from a binary black hole (BH) merger [47], more and more GW signals were detected, including NS mergers [45,46,48,49], which has opened a new window on NS observation by using GWs as probes of their internal structure.

In our previous work [50] we investigated radial oscillations, and found a clear difference of their frequencies between pure NSs and HSs. The radial oscillation of NSs is the simplest oscillation mode without direct GW radiation,

*huanchen@cug.edu.cn

but might couple with and amplify GWs [51,52] and modulate the short gamma ray burst (SGRB) [53].

On the contrary, the nonradial oscillation (NRO) of a star can directly produce GW signals [54], not only in NS mergers or supernova explosions. Therefore, the study of NROs of isolated NSs may provide us with direct and stable observations to understand the structure and properties of high-density NM, the strong interaction, and GWs. In this work we further study the NROs of NSs, specifically the quadrupole oscillations which are stable sources of GW radiation.

The theoretical study of NROs in general relativity was first proposed by Thorne [54,55]. After that, a series of rigorous mathematical analyses were carried out by Detweiler and Lindblom [56,57], whereas Chandrasekhar and Ferrari proposed a simpler calculation and obtained some properties of NROs of compact stars [58]. In recent years, many investigations of NS NROs were carried out, for example, Refs. [59–66]. They show that some eigenfrequencies of the NROs of NSs are within the sensitive range of some current detectors. Theoretically, for a nonrotating NS, the eigenmodes of oscillation are divided into g mode, f mode, and p mode, which indicate the various dominant restoring forces for the perturbations. The g-mode eigenfrequencies are relatively small, $\sim\mathcal{O}(1\ \mathrm{kHz})$, and provide us with an appropriate observable. The buoyancy acts as the g-mode restoring force to bring disturbed fluid elements back into equilibrium, and generally its frequency depends on the particle fraction gradient and temperature [67]. This effect is more intense in HSs than in pure NSs [61,68]. Therefore, we can expect different characteristics of the g modes between NSs and HSs, and we will mainly focus on this mode.

In this work, we adopt the BHF theory for NM, which is based on realistic many-body forces that describe accurately nucleon scattering data in free space and the properties of the deuteron. Moreover, the BHF approach enables the derivation of the properties of NM at nuclear saturation density consistent with experiments [2,6,7,69,70]. For QM, we adopt the Dyson-Schwinger-equation quark model [25,27], which can simultaneously address both confinement and dynamical chiral symmetry breaking [23,24]. We employ the Gibbs phase transition between the hadron and deconfined quark phase [25,71], which determines a range of baryon densities where the hadron and quark phase coexist. In this framework, the maximum masses of the pure NSs and HSs fulfill the two-solar-mass constraint [28–31].

This work is organized as follows. In Sec. II we briefly describe the formalism for the EOSs, i.e., the BHF theory for the hadron phase and the DSEs for the quark phase. In Sec. III we introduce the TOV and the eigenvalue equations for the NROs of NSs. Numerical results are given in Sec. IV, and we draw the conclusions in Sec. V. We use natural units $c = \hbar = 1$ throughout the paper.

II. EQUATION OF STATE

A. Nuclear matter

The BHF many-body theory [72,73] is used to describe the NM in the interior of NSs. It can reproduce NM properties near the saturation density with a quite good accuracy [2,70]. We only provide here a brief overview of the formalism, and refer to the various indicated references for full details. The essential ingredient of this approach is the interaction matrix G, which satisfies the following equations

$$G(\rho, x_p; E) = V + V\sum_{1,2}\frac{|12\rangle(1-n_1)(1-n_2)\langle 12|}{E - e_1 - e_2 + i0}G(\rho, x_p; E) \tag{1}$$

and

$$U_1(\rho, x_p) = \sum_2 n_2\langle 12|G(\rho, x_p; e_1 + e_2)|12\rangle_a, \tag{2}$$

where $n_i(k)$ is a Fermi distribution, $x_p \equiv \rho_p/\rho$ is the proton fraction, and ρ_p and ρ are the proton and the total nucleon number densities, respectively. E is the starting energy and $e_i(k) \equiv k^2/2m_i + \mathrm{Re}U_i(k)$ is the single-particle energy. The multi-indices 1,2 denote in general momentum, isospin, and spin. The energy density of NM can then be expressed as

$$\varepsilon_N = \sum_1 n_1(k)\left(\frac{k^2}{2m_1} + \frac{1}{2}U_1(k)\right). \tag{3}$$

Thus, the nucleon-nucleon interaction potential V is the only necessary input in the calculation process. In this work, we adopt the Argonne V_{18} (V18) [74] and Bonn-B (BOB) [75,76] potentials, supplemented with compatible microscopic three-body forces [5,69,77,78]. This is a common prescription adopted in the BHF approach, and allows us to reproduce correctly the saturation point of symmetric NM and related properties.

In order to obtain the EOS, we impose cold, neutrino-free, charge neutral, and catalyzed matter consisting of neutrons, protons, and leptons (e^-, μ^-) in beta equilibrium due to weak interactions. Therefore, the energy density of NM can be expressed as

$$\varepsilon(\rho_n, \rho_p, \rho_e, \rho_\mu) = (\rho_n m_n + \rho_p m_p) + \varepsilon_N(\rho_n, \rho_p) + \varepsilon_e(\rho_e) + \varepsilon_\mu(\rho_\mu), \tag{4}$$

where $\varepsilon_{e,\mu}$ are the energy densities of electrons and muons, and $m_{n,p}$ are the masses of neutrons and protons, respectively.

Furthermore, a quadratic dependence on the proton fraction is well fulfilled [79–83],

$$\varepsilon_N(\rho_n,\rho_p) = \varepsilon_{\rm SNM}(\rho) + (1-2x_p)^2\varepsilon_{\rm sym}(\rho), \quad (5)$$

being $\varepsilon_{\rm sym}(\rho)$ the symmetry energy density,

$$\varepsilon_{\rm sym}(\rho) = \varepsilon_{\rm PNM}(\rho) - \varepsilon_{\rm SNM}(\rho). \quad (6)$$

Therefore, for the treatment of beta-stable matter, it is only necessary to calculate the energy densities for symmetric nuclear matter (SNM) and pure neutron matter (PNM). For practical use, we employ the convenient empirical parametrizations given in Refs. [8,70]. We have shown in [83] that going beyond the parabolic approximation affects the results for NS structure only in a very marginal way.

The various chemical potentials of the particle species $i = n,\ p,\ e,\ \mu$ can be computed from the energy density, Eq. (4),

$$\mu_i = \frac{\partial\varepsilon}{\partial\rho_i}, \quad (7)$$

and this allows us to solve the equations for beta equilibrium,

$$\mu_p + \mu_e = \mu_n \equiv \mu_B, \qquad \mu_e = \mu_\mu, \quad (8)$$

together with charge neutrality,

$$\rho_p - \rho_e - \rho_\mu \equiv \rho_C = 0, \quad (9)$$

for the equilibrium composition ρ_i at fixed baryon density $\rho_B = \rho = \rho_p + \rho_n$. Finally, the EOS is given by

$$p(\varepsilon) = \rho_B^2 \frac{d}{d\rho_B}\frac{\varepsilon(\rho_i(\rho_B))}{\rho_B} = \rho_B\frac{d\varepsilon}{d\rho_B} - \varepsilon = \rho_B\mu_B - \varepsilon. \quad (10)$$

The BHF approach provides only the EOS for the bulk matter region $\rho \gtrsim 0.1$ fm^{-3} without cluster formation, and therefore it has to be joined with a low-density crust EOS. In this paper we adopt the Shen2020 EOS [84], which belongs to the class of so-called unified EOSs, and is frequently used for the simulations of core-collapse supernova and NS mergers. We notice that the high-mass domain that we are mainly interested in, is in any case hardly affected by the structure of this low-density transition region [82]. The choice of the crust model can influence the predictions of radius and related deformability to a small extent, of the order of 1% for $R_{1.4}$ [82,85,86], which is negligible for our purpose. Even neglecting the crust completely, NS radius and deformability do not change dramatically [87].

Due to the absence of strict theoretical and observational constraints on how to join the core and crust EOSs, we use the simplest way, a continuous transition at the point with the same pressure and energy density. The possible influence of the core-crust transition construction on the NROs will be discussed in following.

B. Quark matter

As in Ref. [88], we adopt the Dyson-Schwinger model (DSM) [25] to describe the deconfined quark phase, which provides a continuous approach to quantum chromodynamics (QCD). The fundamental quantity of the DSM is the quark propagator $S(p;\mu)$ at finite chemical potential μ, which satisfies the Dyson-Schwinger equation

$$S(p;\mu)^{-1} = Z_2[i\boldsymbol{\gamma}\cdot\boldsymbol{p} + i\gamma_4(p_4 + i\mu) + m_q] + \Sigma(p;\mu) \quad (11)$$

with the renormalized self-energy expressed as

$$\Sigma(p;\mu) = Z_1 g^2(\mu) \times \int \frac{d^4q}{(2\pi)^4} D_{\rho\sigma}(k;\mu)\frac{\lambda^a}{2}\gamma_\rho S(q;\mu)\frac{\lambda^a}{2}\Gamma_\sigma(q,p;\mu), \quad (12)$$

where $D_{\rho\sigma}(k \equiv p-q;\mu)$ is the full gluon propagator, $\Gamma_\sigma(q,p;\mu)$ is the full quark-gluon vertex, and Z_1 and Z_2 are the quark-gluon vertex and quark wave function renormalization constants. Moreover, λ^a are the Gell-Mann matrices, and m_q is the current-quark bare mass. Knowing the quark-gluon vertex and gluon propagator, one can solve the equation and obtain the quark propagator. In our work, the so-called rainbow approximation and a chemical-potential-modified Gaussian-type effective interaction [25,88] are adopted; see Ref. [25] for details.

The EOS for cold QM is obtained following Refs. [89,90]. The quark number density, pressure, and energy density for each quark flavor at zero temperature can be computed as

$$\rho_q(\mu_q) = 6\int\frac{d^4p}{(2\pi)^4}{\rm tr}_D[-\gamma_4 S_q(p;\mu_q)], \quad (13)$$

$$p_q(\mu_q) = p_q(\mu_{q,0}) + \int_{\mu_{q,0}}^{\mu_q} d\mu\rho_q(\mu), \quad (14)$$

$$\varepsilon_q(\mu_q) = -p_q(\mu_q) + \mu_q\rho_q(\mu_q). \quad (15)$$

The baryon chemical potential and total baryon number density in the quark phase are

$$\mu_B = \mu_u + 2\mu_d, \quad (16)$$

$$\rho_B = \frac{\rho_u + \rho_d + \rho_s}{3}, \quad (17)$$

and the total pressure and energy density are given by summing contributions from all quark flavors and those from electrons and muons. The pressure of QM at zero density is determined by a phenomenological bag constant [91],

$$B_{\mathrm{DS}} = -\sum_{q=u,d,s} p_q(\mu_{q,0}), \tag{18}$$

which is set to 90 MeV fm^{-3} [26,27,91].

The beta equilibrium and charge neutrality in the pure quark phase are expressed as

$$\mu_d = \mu_u + \mu_e = \mu_u + \mu_\mu = \mu_s, \tag{19}$$

$$\rho_C = \frac{2\rho_u - \rho_d - \rho_s}{3} - \rho_e - \rho_\mu = 0. \tag{20}$$

In this work we adopt the Gibbs construction [25,71] for the phase transition between the hadron phase and quark phase. In combination with the respective beta-equilibrium conditions Eqs. (8) and (19), the chemical and mechanical equilibrium in the mixed phase are expressed as

$$\mu_{B,N} = \mu_{B,Q}, \tag{21}$$

$$\mu_{e,N} = \mu_{e,Q}, \tag{22}$$

$$p_N(\mu_e, \mu_B) = p_Q(\mu_e, \mu_B) = p_M(\mu_e, \mu_B), \tag{23}$$

where the subscripts "N," "Q," and "M" represent NM, QM, and the mixed phase, respectively. In the mixed phase, the local charge neutrality conditions Eqs. (9) and (20) are replaced by the global condition

$$\chi\rho_{C,Q} + (1-\chi)\rho_{C,N} = 0, \tag{24}$$

where χ is the volume fraction of QM in the mixed phase. Consequently, the baryon number density $\rho_{B,M}$ and energy density ε_M of the mixed phase can be determined as

$$\rho_{B,M} = \chi\rho_{B,Q} + (1-\chi)\rho_{B,N}, \tag{25}$$

$$\varepsilon_M = \chi\varepsilon_Q + (1-\chi)\varepsilon_N. \tag{26}$$

Specifically, with the Gibbs construction the baryon number density, energy density, and pressure are continuous inside the HS. In contrast, with the Maxwell construction, the pressure varies continuously, while baryon number density and energy density are generally discontinuous at the hadron-to-quark transition interface [92].

III. NEUTRON STARS

A. Hydrostatic equilibrium structure

The general static spherically-symmetric metric which describes the geometry of a static NS can be written as

$$ds^2 = e^{\nu(r)}dt^2 - e^{\lambda(r)}dr^2 - r^2(d\theta^2 + \sin^2\theta\, d\varphi^2), \tag{27}$$

where $e^{\nu(r)}$ and $e^{\lambda(r)}$ are metric functions. The TOV equations [93,94] obtained from the Einstein field equation for the metric are

$$\frac{dp}{dr} = G\frac{(\varepsilon + p)(m + 4\pi r^3 p)}{r^2(2Gm/r - 1)}, \tag{28}$$

$$\frac{dm}{dr} = 4\pi r^2\varepsilon, \tag{29}$$

and the corresponding metric functions

$$e^{\lambda(r)} = (1 - 2Gm/r)^{-1}, \tag{30}$$

$$\nu(r) = -2G\int_r^\infty dr' \frac{e^{\lambda(r')}}{r'^2}(m + 4\pi r'^3 p). \tag{31}$$

The boundary conditions $m(r=0) = 0$, $p(r=0) = p_c$, and $p(R) = 0$, where p_c is the central pressure, lead to equilibrium configurations in combination with the EOS of the NS matter, thus obtaining radius R and mass $M = m(R)$ of a NS for a given central pressure or density.

B. Nonradial oscillations

Thorne developed a complete theory for NROs of NSs from the Einstein field equations [54]. The perturbation of the fluid in the star is described by the Lagrangian displacement vector ξ^α in terms of the dimensionless perturbation functions $W(r)$ and $V(r)$,

$$\begin{aligned}
\xi^r &= re^{-\lambda/2}WY^l_m e^{i\omega t},\\
\xi^\theta &= -V\partial_\theta Y^l_m e^{i\omega t},\\
\xi^\varphi &= -(\sin\theta)^{-2}V\partial_\varphi Y^l_m e^{i\omega t},
\end{aligned} \tag{32}$$

where $Y^l_m(\theta,\varphi)$ are the usual spherical harmonics, and the eigenvalue $\omega = 2\pi f$ is the frequency of the NRO. The eigenfunctions $W(r)$ and $V(r)$ are determined by the pulsation equations. The full NRO equations can be found in the literature [54,57].

As we mainly focus on the g-mode oscillations, in this work we employ the relativistic Cowling approximation, which disregards the perturbations in the metric [95]. The validity of this approximation has been investigated in Refs. [64,96]. The results show that compared to the full solutions, the deviation of the g-mode frequency is quite small for a NS with canonical mass and increases with increasing mass, up to ~10% at $M = 2.2M_\odot$. As for the other two modes, the approximation yields about 10%–30% accuracy for the f-mode frequencies and about 20% for the p mode. We will explore the limits of the Cowling approximation in future work.

The oscillation equations in Cowling approximation are

$$r\frac{dW}{dr} = \left(\frac{g}{c_s^2} - 3\right)W + e^{\lambda/2}\left(\frac{\omega^2 r^2}{c_s^2 e^{\nu}} - l(l+1)\right)V, \tag{33}$$

$$r\frac{dV}{dr} = e^{\lambda/2}\left(\frac{N^2}{\omega^2} - 1\right)W + \left(2g + \frac{N^2 r^2}{g e^{\nu-\lambda}} - 2\right)V, \tag{34}$$

with $g \equiv -r(dp/dr)/(p+\varepsilon)$, and N being the Brunt-Väisälä (BV) frequency defined as

$$N^2 \equiv \frac{g^2}{r^2}\left(\frac{1}{c_e^2} - \frac{1}{c_s^2}\right)e^{\nu-\lambda}. \tag{35}$$

In the Newtonian approximation N is the frequency of the perturbed fluid elements forced by buoyancy to perform harmonic oscillations.

The BV frequency depends on the difference of the inverse squared equilibrium speed of sound c_e and adiabatic speed of sound c_s, caused by the deviation from beta equilibrium during fast enough oscillations. The former is defined as the derivative of the EOS in beta equilibrium,

$$c_e^2 \equiv \frac{dp/d\rho_B}{d\varepsilon/d\rho_B} = \frac{dp}{d\varepsilon}, \tag{36}$$

while, assuming that all weak reactions are slow compared to the oscillation timescale, the squared adiabatic speed of sound is

$$c_s^2 \equiv \left(\frac{\partial p}{\partial \varepsilon}\right)_{S,Y_i} = \frac{\Delta p}{\Delta \varepsilon}, \tag{37}$$

where S and Y_i denote entropy and the particle fractions affected by weak reactions, respectively. It is related to the adiabatic index of the fluid,

$$\gamma = \left(1 + \frac{\varepsilon}{p}\right)c_s^2, \tag{38}$$

which drives the response of the stellar material to pulsational perturbations.

However, one should note that Eq. (37) is only adequate in the pure hadron/quark phases. In the mixed phase, one also needs to consider the transition between NM and QM, as well as the independent expansion/contraction of NM/QM during the oscillation. The related conversion rate/timescale between hadron and quark phases is still an open question, and current calculations are model dependent. Following the argument of [97], the preferred conversion timescale would be slow at the hadron-quark interface, although a rapid timescale cannot be discarded [98,99].

Therefore, herein we neglect the phase transition between NM and QM during the oscillation of the mixed phase. At the timescale of oscillations, fluid elements expand or compress while keeping all particle fractions Y_i constant in NM and QM separately. Note that this means that the strong chemical equilibrium between NM and QM is violated, i.e., the isospin chemical potentials in NM and QM are different during oscillations. The volume fraction of QM in the mixed phase changes during the oscillation, to keep the pressure equilibrium between NM and QM. Accordingly, the squared adiabatic speed of sound in the mixed phase is modified as [61]

$$c_s^{-2} = \frac{\chi'\varepsilon'_Q + (1-\chi')\varepsilon'_N - \varepsilon}{p' - p}, \tag{39}$$

where p and ε are the pressure and energy density in beta equilibrium, $p' = p + \Delta p$ is the pressure during oscillations, ε'_Q, ε'_N are the energy densities of QM and NM during oscillations, and χ' is determined by $p'_Q = p'_N = p'$ during oscillations.

In this work, we focus on the influence of the core on the NROs, as in recent literature [61,63,64]. For simplification, we will make the approximation that $c_s = c_e$ in the crust, and, correspondingly, the BV frequency $N_{\rm crust} = 0$. The influence of the crustal N on the core modes of NROs is small, which will be discussed in the following section.

In order to determine the eigenfrequencies of oscillation, one also needs boundary conditions [100], which, in the NS center, are given by

$$W(0) + lV(0) = 0, \tag{40}$$

while at the outer surface of the star, the Lagrangian perturbation of the pressure should vanish,

$$\Delta p(R) = \gamma p\left[-e^{-\lambda/2}\left(r\frac{dW}{dr} + 3W\right) - l(l+1)V\right](R) = 0. \tag{41}$$

Due to the homogeneousness of the oscillation equations (33) and (34), one can impose arbitrarily $W(r=0) = 1$ and $V(r=0) = -1/2$ at the center. Then integrating Eqs. (33) and (34) from center to the surface with the boundary conditions yields the discrete eigenfrequencies ω_i and the eigenfunctions W_i, V_i. For the quadrupole ($l = 2$) oscillations of pure NSs and HSs, they can be ordered as $\omega_{g_n} < \ldots < \omega_{g_1} < \omega_f < \omega_{p_1} < \ldots < \omega_{p_n}$, where n is the number of nodes.

C. GW damping time

The full solution of the NRO equations produces complex oscillation frequencies of quasinormal modes, the imaginary part being related to the damping time. In the Cowling approximation the oscillation frequencies are instead purely real, because the response of the metric to fluid perturbations is neglected. In this work, similar to

Refs. [62,67,100,101], we combine the Newtonian approximation for the oscillation energy with the lowest-order post-Newtonian quadrupole formula for the gravitational wave radiation in order to estimate the GW damping time. Accordingly, the damping time of oscillations through GW emission is

$$\tau_{\rm GW} = \frac{2E}{P_{\rm GW}}, \tag{42}$$

where E is the total energy stored in the oscillation, and $P_{\rm GW}$ is the power of the GW radiation released by the mode.

The energy per radial distance of an eigenmode in Cowling approximation is given by [100]

$$\frac{dE}{dr} = \frac{\omega^2}{2}(p+\varepsilon)e^{(\lambda-\nu)/2}r^4[W^2 + l(l+1)V^2], \tag{43}$$

and its power, involving weak field approximation and slow motion approximation, $\omega R \ll 1$, can be estimated as [67,100]

$$P_{\rm GW} = \frac{G(l+1)(l+2)}{8\pi(l-1)l}\left[\frac{4\pi\omega^{l+1}}{(2l+1)!!}\int_0^R dr r^{l+2}\delta\epsilon\right]^2, \tag{44}$$

where $\delta\epsilon$ is the Eulerian perturbation of the energy density,

$$\delta\epsilon = -(p+\varepsilon)\left[e^{-\lambda/2}\left(3W + r\frac{dW}{dr}\right) + l(l+1)V\right] - r\frac{d\varepsilon}{dr}e^{-\lambda/2}W. \tag{45}$$

It has been pointed out [67] that the different terms in this equation are of different signs and tend to cancel each other, which renders a reliable numerical evaluation very delicate. We will come back to this problem later.

The radiation power is related to the GW strain (metric perturbation), which in quadrupole approximation and transverse-traceless (TT) gauge is [102,103]

$$h_{ij}^{\rm TT}(t,D) = \frac{2G}{D}\ddot{Q}_{ij}^{\rm TT}(t - D/c), \tag{46}$$

where $i, j = 1, 2, 3$ are the indices in Cartesian coordinates, D is the distance to the source, G is the gravitational constant, the two dots represent the second time derivative, and the traceless quadrupole moment is

$$Q_{ij}^{\rm TT}(t) = \int d^3\boldsymbol{x}\varepsilon(t,\boldsymbol{x})\left(x_i x_j - \frac{1}{3}\delta_{ij}|\boldsymbol{x}|^2\right). \tag{47}$$

The metric perturbation tensor can be decomposed as

$$\mathbf{h}^{\rm TT} = h_+\mathbf{e}_+ + h_\times\mathbf{e}_\times, \tag{48}$$

where $\mathbf{e}_+$ and $\mathbf{e}_\times$ are the unit tensors of plus and cross polarization.

In the case of a symmetric metric, the cross polarization $h_\times$ is zero, Q_{ij} has only diagonal components $Q_{11} = Q_{22} = -\frac{1}{2}Q_{33}$, and the GW strain can be calculated by [104]

$$h_+ = \frac{3G\sin^2\alpha}{2D}\ddot{Q}_{33}, \tag{49}$$

where α is the inclination angle. In this work, we choose $\sin\alpha = 1$. After some derivation, $\ddot{Q}_{33}$ can be written as

$$\ddot{Q}_{33} = |\ddot{Q}_{33}|e^{-i\omega t} = \int dr r^2 \sin\theta d\theta d\varphi r^2\left(\sin^2\theta - \frac{1}{3}\right)\frac{d^2\delta\epsilon}{dt^2}, \tag{50}$$

and thus

$$|\ddot{Q}_{33}| = \frac{4\sqrt{\pi/5}}{3}\omega^2\int dr r^4\delta\epsilon(r), \tag{51}$$

where $\delta\epsilon$ is given by Eq. (45). So the amplitude of the GW strain can be rewritten as

$$|h_+| = \frac{3G|\ddot{Q}_{33}|}{2D}, \tag{52}$$

and depends, as the radiation power, on $\delta\epsilon(r)$.

IV. NUMERICAL RESULTS

A. EOS and equilibrium structure of neutron stars

As discussed above, we use the BHF EOS with BOB or V18 potential for the pure NM. Regarding the QM EOS in HSs, there is a free model parameter α, which represents the strength of the in-medium modification of the Gaussian-type effective interaction in the DSM. Here we choose $\alpha = 1, 2$ and $\alpha = 1, 1.5$ in combination with the BHF BOB and V18 EOSs, respectively, labeled as BOB/V18 + DSα, to satisfy both the requirements of $M_{\rm max} > 2M_\odot$ and causality, as discussed in detail in [25,88].

The energy density, squared equilibrium speed of sound, and squared adiabatic speed of sound as functions of the pressure are shown in Fig. 1. The colors/types of curves refer to the different combinations of BHF and DSM EOS. The EOS of the mixed phase (broken curves) is generally softer than that of the pure NM (solid curves), whereas pure QM emerges at too high densities that cannot be reached in HSs in our approach. However, the QM onset density is strongly dependent on the theoretical model adopted for the description of QM.

We notice that both sound speeds in pure NM become superluminal at high densities (but quite close to the $M_{\rm max}$ configuration), due to the nonrelativistic character of the

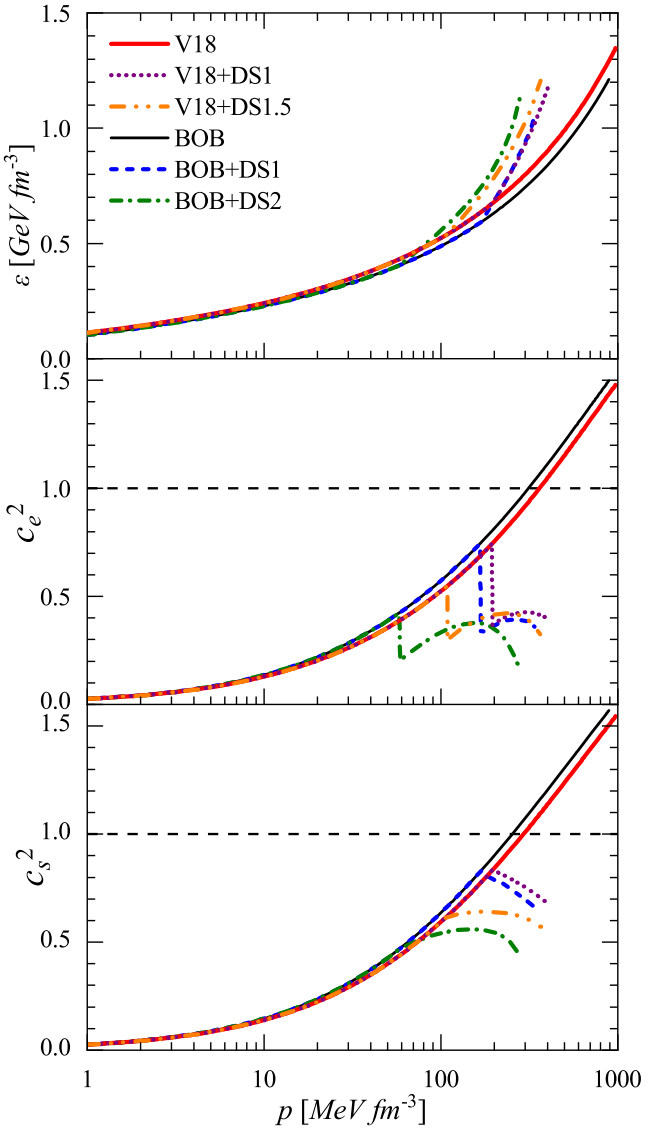

FIG. 1. The energy density (upper panel), squared equilibrium speed of sound (central panel), and squared adiabatic speed of sound (lower panel) of NS matter as functions of pressure with different EOSs. All curves end at the $M_{\max}$ configuration for the proper EOS. See the text for a detailed description of the notation.

BHF theory. However, in our model, the phase transition to QM occurs always at lower density, and consequently causality is never violated. The equilibrium speed of sound c_e is particularly sensitive to the composition of the matter. One can find a small discontinuity at $p \approx 5$ MeV fm^{-3} due to the onset of muons (hardly visible because of the scale), and a sharp discontinuous drop at the phase transition point, due to the appearance of QM. Unlike c_e, the adiabatic speed of sound c_s is always continuous with increasing pressure, regardless of the emergence of muons or quarks. This is because it is defined with fixed particle composition, Eq. (37). Similar results were obtained in Ref. [64], using different NM and QM EOSs.

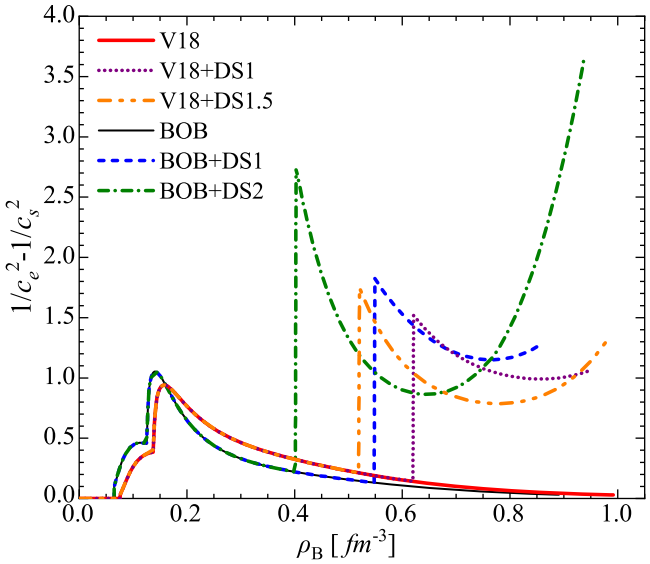

FIG. 2. Difference of squared inverse sound speeds $1/c_e^2 - 1/c_s^2$ vs baryon number density. All curves end at the $M_{\max}$ configuration for the proper EOS.

In Fig. 2 we show the difference of squared inverse sound speeds $1/c_e^2 - 1/c_s^2$ as a function of the baryon number density in NS matter. This difference determines the profile of the local oscillation frequency, i.e., the BV frequency, Eq. (35). As discussed above, we approximate $c_s = c_e$ and $N = 0$ in the crust, therefore the difference is zero below the core-crust transition density. In the core with the pure BHF EOS, c_s and c_e increase with density, and therefore $1/c_e^2 - 1/c_s^2$ decreases. There is a first spike around $\rho_B \simeq 0.15$ fm^{-3} due to the muon onset, and at larger densities a second much sharper spike due to the appearance of QM. In the mixed phase the difference decreases and then increases again when approaching the pure quark phase. We stress that the (sharp) change of $1/c_e^2 - 1/c_s^2$ is mainly due to the (sharp) change of c_e, which is very sensitive to the change of particle species, see Fig. 1.

Furthermore we notice that, whereas the sound speed differences in the purely hadronic phase become very small and rapidly approach zero, those in the mixed phase are larger and can rise very quickly. This behavior already hints at larger values of the g-mode frequencies and a strong dependence on the QM EOS in hybrid stars compared to the purely hadronic stellar configurations. However, the appearance of hyperons [105,106] or superfluidity [105,107–109] can also lead to such sharp changes, and cause an increase of the g-mode frequency, which would thus not be a sufficient indication for the presence of QM.

The mass-radius relations of pure NSs and HSs with the various considered EOSs are shown in Fig. 3. The broken curve segments indicate the hybrid star branches. One notes that the differences between HSs and pure NSs are even smaller than the differences between pure NSs with different BHF EOSs. Therefore, it is difficult to distinguish HSs

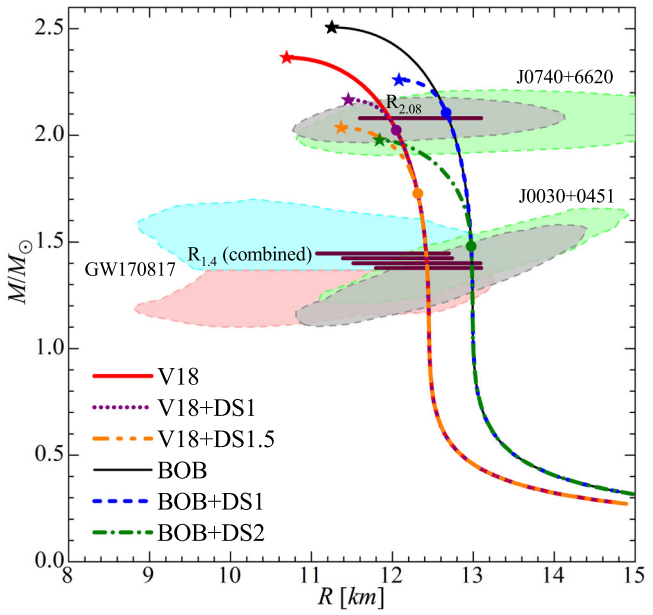

FIG. 3. The mass-radius relations of NSs obtained with different EOSs. Full dots indicate the bifurcation points of pure NSs and HSs. The horizontal black bars indicate the limits on $R_{2.08}$ and $R_{1.4}$ obtained in the combined NICER+GW170817 data analyses of [40,42,43]. The maximum-mass configurations are indicated by star symbols.

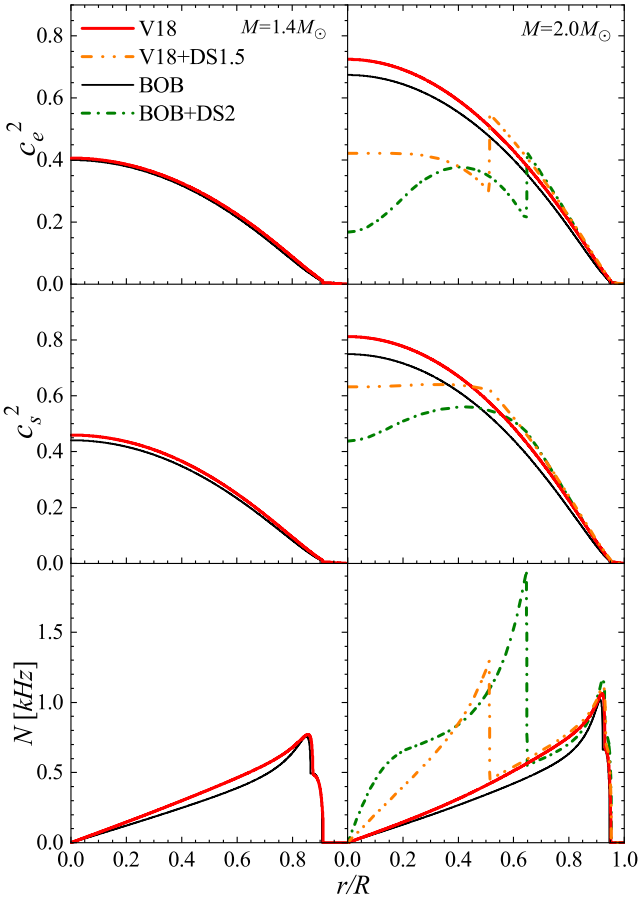

FIG. 4. Squared equilibrium speed of sound (upper panels), squared adiabatic speed of sound (central panels), and BV frequency N (lower panels) in NSs with $1.4M_\odot$ (left panels) and $2.0M_\odot$ (right panels), for various EOSs.

from pure NSs with only $M(R)$ observations. Within our model, pure QM matter does not appear in the core of HSs.

All plotted EOSs (in particular the V18 models) fulfill the constraints from present observations on NS mass and radius, in particular the recent mass-radius results of the NICER mission for the pulsars J0030 + 0451 [37,38] and J0740 + 6620 [40–43]. The combined (strongly model-dependent) analysis of both pulsars together with the GW170817 event observations [45,110] yields improved limits on the radius $R_{2.08} = 12.35 \pm 0.75$ km [40], but, in particular, on $R_{1.4}$, namely, 12.45 ± 0.65 km [40], $11.94^{+0.76}_{-0.87}$ km [42], and $12.33^{+0.76}_{-0.81}$ km or $12.18^{+0.56}_{-0.79}$ km [43], which are shown as horizontal black bars in the figure. The BHF V18 EOS is well compatible with these constraints [2,50,70], and also its maximum mass $M_{\max} \approx 2.36M_\odot$ exceeds the currently known lower limits. The BOB EOS is stiffer and allows a maximum mass of even $2.51M_\odot$. Some theoretical analyses of the GW170817 event indicate also an upper limit on the maximum mass of ~ 2.2–$2.4M_\odot$ [32–35,111], with which the V18 EOS would be compatible as well. However, those are very model dependent, in particular the still to-be-determined temperature dependence of the EOS [9,112–114].

In Fig. 4 we show the profiles of both the equilibrium and adiabatic squared speed of sound, and the BV frequency in NSs with masses $M = 1.4, 2.0M_\odot$ for different EOSs. The speed of sound generally increases from the crust to the center of the NS, apart from the density region close to the pure quark phase or a sudden drop of c_e due to the onset of QM (e.g., upper right panel), which does not take place in the $1.4M_\odot$ configurations shown in the left panels. By definition, the BV frequency vanishes in the center and increases towards the crust, exhibiting sharp decreases at the phase transition point or when muons disappear. We see that in the inner core of HSs, the BV frequency is much larger than in pure NSs. The BV frequency is a local property in NSs which cannot be observed directly, but it is closely related to the global g-mode frequency. Accordingly, one can consider the BV frequency and the g-mode oscillations as useful probes of the appearance of QM. We will discuss this in detail now.

B. Nonradial oscillations of neutron stars

In this work, we investigate the quadrupole oscillations ($l = 2$) of both pure NSs and HSs. For illustration, we show some typical solutions for the radial and tangential displacement perturbations $W(r)$ and $V(r)$ in Fig. 5. The left panels contain the results of four representative f, g_1, g_2, and p_1 eigenmodes of a $1.4M_\odot$ NS with the V18 EOS,

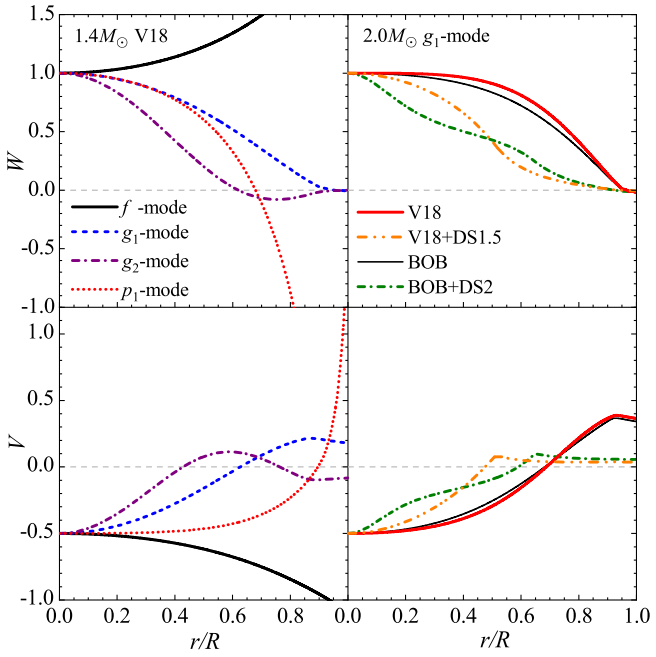

FIG. 5. The radial displacement perturbation W (upper panels) and the tangential displacement perturbation V (lower panels) of the first four eigenmodes of NROs for a $1.4M_\odot$ NS with the $V18$ EOS (left panels) and of the g_1 mode for a $2.0M_\odot$ NS with various EOSs (right panels).

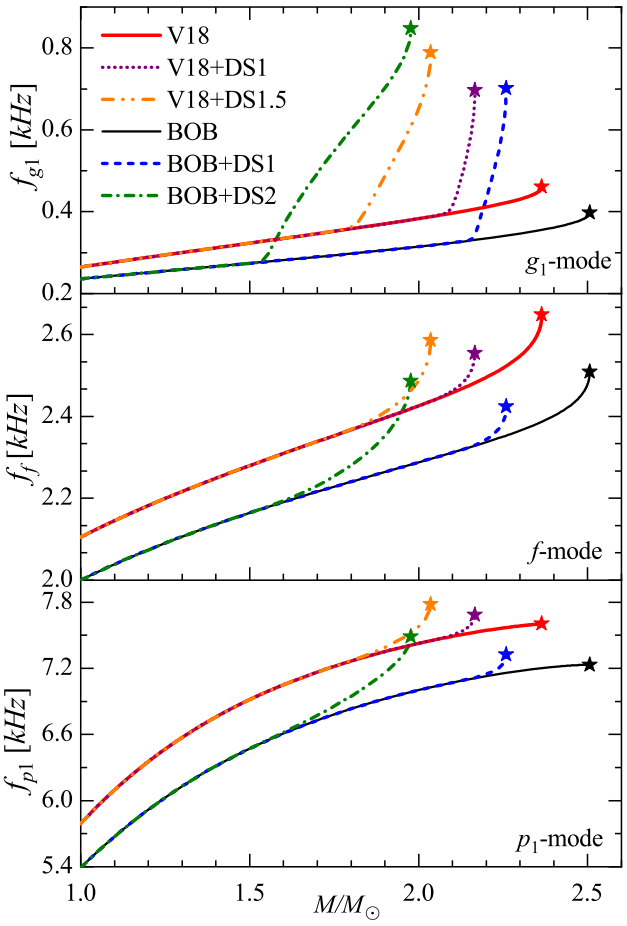

FIG. 6. g_1-, f-, and p_1-mode frequencies vs mass M for various EOSs.

exhibiting the expected number of nodes, whereas the right panel displays the g_1 mode of $2.0M_\odot$ NSs with various EOSs. In this case, for purely hadronic NSs (solid curves), one can see quite similar oscillation amplitudes nearly independent of the nuclear EOS, whereas the amplitudes in HSs (broken curves) decrease more quickly in the inner core and remain smaller in the outer layers. Therefore, the oscillation in HSs occurs mainly in the inner core, and might reveal information about the QM/mixed phase. The $W(r)$ eigenfunction exhibits a smooth behavior over the entire star's profile, even at the radial distance corresponding to the mixed phase onset; this is at variance with $V(r)$, which shows sudden kinks when QM appears.

Now we turn to the discussion of the NRO frequencies in NSs and HSs, for the g, f, and p modes. As known, they are classified according to the different restoring forces acting in the fluid, and are characterized by different frequencies. In Fig. 6, we show the NRO frequencies of NSs as functions of NS mass. One can see that f_{g_1} of pure NSs lies in the range 0.2–0.4 kHz, and increases slowly with the NS mass. The difference of the eigenfrequencies with BOB and V18 EOSs is always about 0.1 kHz, which is related to the corresponding difference of the BV frequencies, Fig. 4, and, in particular, to the different NS radii, Fig. 3: the smaller V18 star is oscillating faster. The same qualitative correlations are observed for the HSs, which exhibit much higher eigenfrequencies up to 0.9 kHz. Therefore f_{g_1} might be a good observable to distinguish HSs from pure NSs. Again, our results are similar to those discussed in Refs. [61,64,68].

Equivalent features are observed for the much higher eigenfrequencies of f mode and p_1 mode, above 2 and 6 kHz, respectively. But in this case, the differences between HSs and pure NSs are not larger than the difference between pure NSs with different models. Therefore, they cannot be used as good observables to distinguish HSs from purely hadronic NSs.

The eigenfrequencies of several representative modes of NSs with $M = 1.4, 2.0M_\odot$ and various EOSs are also listed in Table I. One can see that the frequencies of higher-order g modes decrease and those of higher-order p modes increase with order. These results are qualitatively similar to those recently published in Refs. [61,62].

C. GW emission and damping of g_1 mode

In the previous section, we pointed out the significant difference of the g-mode frequencies between massive NSs and HSs. In the following, we investigate a closely related observable, the damping time of oscillations through GW emission, Eq. (42). Before illustrating the results,

TABLE I. The NRO frequencies f (in units of kHz) of six representative eigenmodes of NSs with $M = 1.4, 2.0M_\odot$ and various EOSs.

	$1.4M_\odot$		$2.0M_\odot$			
Mode	V18	BOB	V18	V18 + DS1.5	BOB	BOB + DS2
g_3	0.15	0.13	0.19	0.33	0.16	0.44
g_2	0.20	0.18	0.25	0.39	0.21	0.57
g_1	0.31	0.27	0.38	0.65	0.31	0.85
f	2.25	2.14	2.43	2.49	2.29	2.49
p_1	6.77	6.33	7.43	7.58	7.00	7.49
p_2	8.74	8.21	10.59	10.78	9.88	10.48

we remind that three possible damping mechanisms can act on g-mode oscillations, i.e., relaxation toward chemical equilibrium, viscous damping, and damping due to emission of GWs. In Ref. [67] damping times of the core g modes (as well as of crustal discontinuity g modes) of order 10^8–10^{11} s were obtained (but are subject to delicate numerical cancellations). Thus damping due to emission of GWs is very inefficient, and the other mechanisms are dominant.

Our results are shown in Fig. 7(a) for g_1-mode oscillations with various EOSs as a function of NS mass. In the low-mass region ($\lesssim 1.4M_\odot$), we obtain also very large values of the damping time, and even a divergence at certain masses. This large value of $\tau_{\rm GW}$ is due to the

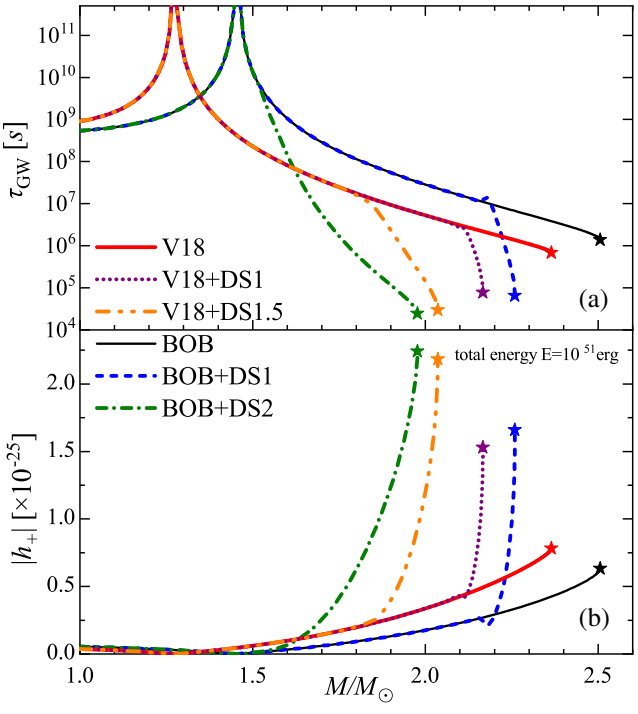

FIG. 7. Properties of g_1-mode oscillations vs NS mass M for various EOSs: (a) The damping time and (b) the amplitude of the GW strain $|h_+|$ for a total GW energy $E = 10^{51}$ erg and distance $D = 15$ Mpc.

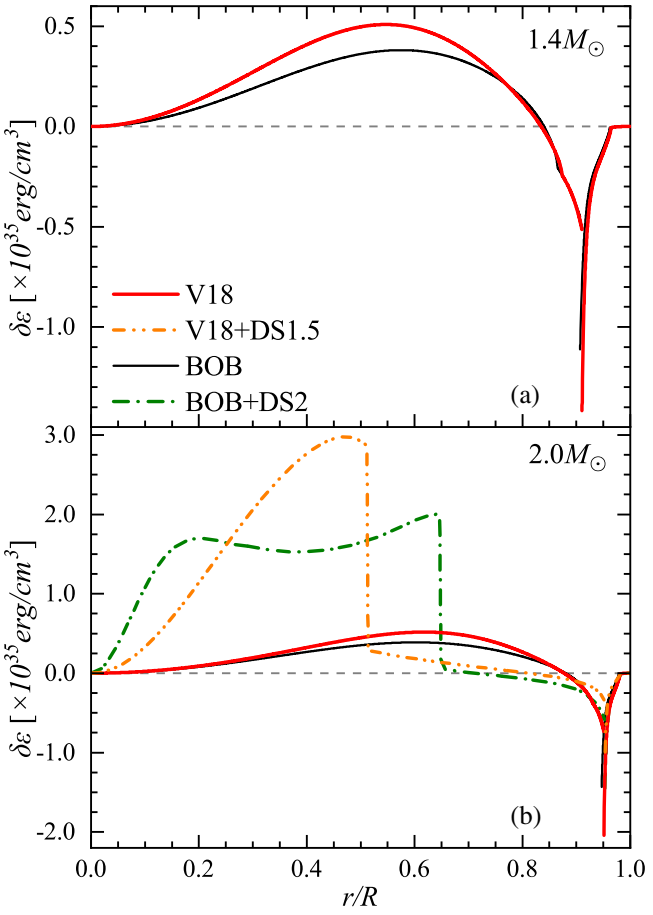

FIG. 8. Eulerian perturbation of the energy density, Eq. (45), in NSs with $1.4M_\odot$ (a) and $2.0M_\odot$ (b) for various EOSs. The normalization is as in Fig. 7.

smallness of the integral for the GW power, Eq. (44), caused by cancellations between the individual terms of Eq. (45). The integral represents a superposition of GWs emitted from perturbations of the energy quadruple moment at different layers of the NS.

This is illustrated in Fig. 8, which shows the Eulerian perturbation of the energy density, $\delta\epsilon(r)$, Eq. (45), in $1.4M_\odot$ and $2.0M_\odot$ NSs. Similar to the perturbation functions $W(r)$ and $V(r)$, the perturbation of the energy (quadruple moment) also has nodes at certain radii. The sign flip of $\delta\epsilon$ represents a half-period difference of the oscillation phase of the energy quadruple moment. Therefore the GWs emitted from domains with different signs of $\delta\epsilon$ will interfere with each other, which results in cancellations of the power output. In our models, we obtain contributions of positive $\delta\epsilon$ in the inner core and negative $\delta\epsilon$ in the outer layers of the same order of magnitude. As a result, we obtain large values of the damping time $\tau_{\rm GW}$, and even a divergence at a certain mass. We stress that the (small) values of the GW power are quite model dependent, which could be greatly influenced by various approximations, and so do the values of the damping time $\tau_{\rm GW}$ [67].

TABLE II. The minimum detectable energy $E_{\rm GW}$, Eq. (53), (in units of erg) of $M = 1.4, 2.0M_\odot$ NSs at two representative distances for various EOSs.

		$1.4M_\odot$		$2.0M_\odot$			
Detector	Distance	V18	BOB	V18	V18 + DS1.5	BOB	BOB + DS2
LIGO/Virgo	10 kpc	1.5×10^{46}	1.1×10^{46}	2.3×10^{46}	6.8×10^{46}	1.6×10^{46}	1.1×10^{47}
LIGO/Virgo	15 Mpc	3.5×10^{52}	2.5×10^{52}	5.2×10^{52}	1.5×10^{53}	3.5×10^{52}	2.6×10^{53}
Einstein	10 kpc	6.2×10^{44}	4.5×10^{44}	9.3×10^{44}	2.7×10^{45}	6.3×10^{44}	4.6×10^{45}
Einstein	15 Mpc	1.4×10^{51}	1.0×10^{51}	2.1×10^{51}	6.1×10^{51}	1.4×10^{51}	1.0×10^{52}

Figure 8(b) shows that for massive pure NSs the positive contribution in the inner core is dominant, and thus the damping time in Fig. 7(a) is about 10^6–10^8 s (∼days), and decreases with the NS mass. This means that the g_1 mode of a pure NS is likely to be a stable and long-lasting source of GWs, if no other very strong damping mechanisms dominate. But for the hybrid stars, the positive contributions of $\delta\epsilon$ in the inner core are much larger, and the damping time decreases very quickly by several orders of magnitude with respect to pure NSs. Thus the behavior of the g_1-mode GW damping time shows again a significant difference between HSs and pure NSs, just like the frequencies.

The much smaller damping time of HSs indicates a much stronger GW strain $|h_+|$, Eq. (52). This quantity depends on the oscillation amplitudes W and V. Their normalization can be determined from the total energy E of oscillation through Eq. (43). Choosing a typical energy scale $E \sim 10^{51}$ erg [97] and a typical distance $D \sim 15$ Mpc (star in the Virgo cluster), we show in Fig. 7(b) the GW strain amplitude of NS and HS g_1-mode oscillations. One can see that $|h_+|$ for pure NSs with low masses is much lower, with even a zero point, which corresponds to the high damping time and its divergence in the upper panel. For NSs with larger masses, $|h_+|$ increases with the NS mass, while for HSs the equivalent irregular behavior as for $\tau_{\rm GW}$ is exhibited. Therefore, our results for both the damping time and the strain amplitude suggest stronger GW g_1-mode radiation of HSs than pure NSs, which could thus be good observables to distinguish those from each other.

D. Prospects of observation

Some of these features are likely to be detected by the next generation of GW detectors [115], while the frequencies of f and p modes are not in the range of sensitivity of current ground-based detectors. Although the GW strain emitted by NSs in the Virgo cluster is only of the order 10^{-25}, a $|h_+|$ of the order 10^{-22} could be obtained for NSs in our galaxy ($D \sim 10$ kpc), which is within the detection ability of present GW detectors. The minimum energy that should be released to be detectable in present and planned GW observatories can be estimated as [116,117]:

$$\frac{E_{\rm GW}}{M_\odot} = 3.5 \times 10^{36} \frac{1+4Q^2}{4Q^2} \frac{S_n}{1\ \mathrm{s}} \left(\frac{S}{N} \frac{D}{10\ \mathrm{kpc}} \frac{f}{1\ \mathrm{kHz}} \right)^2, \quad (53)$$

where $Q = \pi f \tau_{\rm GW}$ is the quality factor, S_n is the noise power spectral density of the detector, and S/N is the signal-to-noise ratio.

Table II lists some representative values, for typical distances $D = 10$ kpc (star in our galaxy) and $D = 15$ Mpc (star in the Virgo cluster), taking $S/N = 8$ and $S_n^{1/2} = 2 \times 10^{-23}$ s$^{1/2}$ (representative of Advanced LIGO/Virgo at ∼kHz frequency [45]), and $S_n^{1/2} = 10^{-24}$ s$^{1/2}$ (illustrative of the planned third-generation ground-based Einstein Observatory at the same frequencies [118]). Although the minimum detectable energy of NSs in the Virgo cluster is of the order 10^{52}–10^{53} erg, higher than the typical energy that can be released by a NRO g mode, the threshold for stars in our galaxy is only 10^{46}–10^{47} erg, much lower than this typical energy. Therefore, those events could be detected by present and planned GW observatories.

V. CONCLUSIONS

In this work we investigated non-radial quadrupole oscillations of cold and isolated NSs, including pure NSs and HSs. We adopted the BHF theory for NM, the DSM for QM, and the Gibbs construction for their phase transition. Based on the equilibrium structure, we solved the equations for the non-radial $l = 2$ oscillations within Cowling approximation, and obtained the radial and tangential displacement perturbations in NSs as well as the eigenfrequencies of g, f, and p modes for various EOSs.

The emergence of QM influences strongly the two kinds of sound speed and the BV frequencies in HSs, and consequently their g-mode oscillations. We find eigenfrequencies $f_{g_1} \sim 300$ Hz for pure NSs, which increase very slowly with the NS mass, while those of HSs increase very quickly, reaching above 700 Hz. All these frequencies are in the sensitivity range of current ground-based GW detectors. This shows a clear difference of the g-mode frequency between pure NSs and HSs, which can thus be a good observable to distinguish them. Such a difference is not obvious for the f and p modes.

The concurrent shorter g_1 damping times of HSs correspond to larger GW strain and radiation power, and thus easier detection than for pure NSs. Estimates of the GW strain h_+ and minimum detectable energy $E_{\rm GW}$ suggest that the GWs from the NRO g_1 mode of NSs/HSs in our galaxy

could be detected by present and planned detectors. To sum up, the g_1 mode is the most suitable mode to provide a window on the internal composition of the compact object. However, besides quark matter, appearance of other kinds of matter such as hyperons and superfluidity in the cores of NSs will cause similar effects on the g-mode frequencies [105–109], and thus make the unique identification of QM difficult. This is worth further investigation in the future.

In this work we disregarded the contribution of the crust to the g-mode oscillations by using the approximation $N_{\rm crust} = 0$. In Ref. [67] the coupling between core and crust NRO modes has been carefully analyzed and their mutual interference was found sufficiently small, i.e., the frequency and damping time of the core modes are only weakly influenced by the crust contribution, especially for high-mass stars. We have confirmed this conclusion by calculations involving the Shen-EOS $N_{\rm crust}$, which will be the subject of a separate paper.

The accurate computation of this feature requires in particular a careful treatment of density discontinuities due to changes of the chemical composition. This might occur inside the crust [119], at the core-crust boundary, or at the critical point from HM to QM with a Maxwell phase transition [65,98,120,121]. The associated discontinuity g modes might have similar eigenfrequencies as and thus mix with the core modes [65,67].

Apart from cold isolated NSs, quadrupole oscillations also occur in various newly born NSs, after NS mergers or supernova explosions, which are expected to be more energetic and easier observable. In such newly born NSs, one needs to consider more realistic environment effects, such as the EOS at finite temperature [100,119], the temperature/entropy distribution in NSs, the neutrino trapping effects, and also rotation. We leave these to future work.

ACKNOWLEDGMENTS

We acknowledge financial support from the National Natural Science Foundation of China—Grant No. 12205260.

[1] E. Annala, T. Gorda, A. Kurkela, J. Nättilä, and A. Vuorinen, Nat. Phys. **16**, 907 (2020).
[2] G. F. Burgio, H.-J. Schulze, I. Vidaña, and J.-B. Wei, Prog. Part. Nucl. Phys. **120**, 103879 (2021).
[3] P. Ring, Prog. Part. Nucl. Phys. **37**, 193 (1996).
[4] A. Y. Potekhin, A. F. Fantina, N. Chamel, J. M. Pearson, and S. Goriely, Astron. Astrophys. **560**, A48 (2013).
[5] Z. H. Li and H.-J. Schulze, Phys. Rev. C **78**, 028801 (2008).
[6] M. Kohno, Phys. Rev. C **88**, 064005 (2013).
[7] K. Fukukawa, M. Baldo, G. F. Burgio, L. Lo Monaco, and H.-J. Schulze, Phys. Rev. C **92**, 065802 (2015).
[8] J. J. Lu, Z. H. Li, G. F. Burgio, A. Figura, and H.-J. Schulze, Phys. Rev. C **100**, 054335 (2019).
[9] H.-M. Liu, J. Zhang, Z.-H. Li, J.-B. Wei, G. F. Burgio, and H.-J. Schulze, Phys. Rev. C **106**, 025801 (2022).
[10] A. Akmal, V. R. Pandharipande, and D. G. Ravenhall, Phys. Rev. C **58**, 1804 (1998).
[11] A. Carbone, A. Polls, and A. Rios, Phys. Rev. C **88**, 044302 (2013).
[12] K. Hebeler, S. K. Bogner, R. J. Furnstahl, A. Nogga, and A. Schwenk, Phys. Rev. C **83**, 031301(R) (2011).
[13] L. Coraggio, J. W. Holt, N. Itaco, R. Machleidt, L. E. Marcucci, and F. Sammarruca, Phys. Rev. C **89**, 044321 (2014).
[14] C. Wellenhofer, J. W. Holt, N. Kaiser, and W. Weise, Phys. Rev. C **89**, 064009 (2014).
[15] C. Drischler, K. Hebeler, and A. Schwenk, Phys. Rev. C **93**, 054314 (2016).
[16] A. Chodos, R. L. Jaffe, K. Johnson, C. B. Thorn, and V. F. Weisskopf, Phys. Rev. D **9**, 3471 (1974).
[17] M. Buballa, Phys. Rep. **407**, 205 (2005).
[18] T. Klähn, R. Lastowiecki, and D. B. Blaschke, Phys. Rev. D **88**, 085001 (2013).
[19] T. Klähn and T. Fischer, Astrophys. J. **810**, 134 (2015).
[20] A. Kurkela, P. Romatschke, and A. Vuorinen, Phys. Rev. D **81**, 105021 (2010).
[21] E. S. Fraga, A. Kurkela, and A. Vuorinen, Astrophys. J. **781**, L25 (2014).
[22] J. C. Jiménez and E. S. Fraga, Phys. Rev. D **100**, 114041 (2019).
[23] C. D. Roberts and A. G. Williams, Prog. Part. Nucl. Phys. **33**, 477 (1994).
[24] R. Alkofer and L. von Smekal, Phys. Rep. **353**, 281 (2001).
[25] H. Chen, M. Baldo, G. F. Burgio, and H.-J. Schulze, Phys. Rev. D **84**, 105023 (2011).
[26] H. Chen, M. Baldo, G. F. Burgio, and H.-J. Schulze, Phys. Rev. D **86**, 045006 (2012).
[27] H. Chen, J. B. Wei, M. Baldo, G. F. Burgio, and H.-J. Schulze, Phys. Rev. D **91**, 105002 (2015).
[28] P. B. Demorest, T. Pennucci, S. M. Ransom, M. S. Roberts, and J. W. Hessels, Nature (London) **467**, 1081 (2010).
[29] J. Antoniadis *et al.*, Science **340**, 1233232 (2013).
[30] E. Fonseca *et al.*, Astrophys. J. **832**, 167 (2016).
[31] H. T. Cromartie *et al.* (NANOGrav Collaboration), Nat. Astron. **4**, 72 (2019).
[32] M. Shibata, S. Fujibayashi, K. Hotokezaka, K. Kiuchi, K. Kyutoku, Y. Sekiguchi, and M. Tanaka, Phys. Rev. D **96**, 123012 (2017).
[33] B. Margalit and B. D. Metzger, Astrophys. J. Lett. **850**, L19 (2017).
[34] L. Rezzolla, E. R. Most, and L. R. Weih, Astrophys. J. Lett. **852**, L25 (2018).

[35] M. Shibata, E. Zhou, K. Kiuchi, and S. Fujibayashi, Phys. Rev. D **100**, 023015 (2019).
[36] D.-S. Shao, S.-P. Tang, X. Sheng, J.-L. Jiang, Y.-Z. Wang, Z.-P. Jin, Y.-Z. Fan, and D.-M. Wei, Phys. Rev. D **101**, 063029 (2020).
[37] T. E. Riley *et al.*, Astrophys. J. **887**, L21 (2019).
[38] M. C. Miller *et al.*, Astrophys. J. **887**, L24 (2019).
[39] E. Fonseca *et al.*, Astrophys. J. Lett. **915**, L12 (2021).
[40] M. C. Miller *et al.*, Astrophys. J. Lett. **918**, L28 (2021).
[41] T. E. Riley *et al.*, Astrophys. J. Lett. **918**, L27 (2021).
[42] P. T. H. Pang, I. Tews, M. W. Coughlin, M. Bulla, C. Van Den Broeck, and T. Dietrich, Astrophys. J. **922**, 14 (2021).
[43] G. Raaijmakers, S. K. Greif, K. Hebeler, T. Hinderer, S. Nissanke, A. Schwenk, T. E. Riley, A. L. Watts, J. M. Lattimer, and W. C. G. Ho, Astrophys. J. Lett. **918**, L29 (2021).
[44] M. Alford, M. Braby, M. Paris, and S. Reddy, Astrophys. J. **629**, 969 (2005).
[45] B. P. Abbott *et al.* (LIGO Scientific, Virgo Collaborations), Phys. Rev. Lett. **119**, 161101 (2017).
[46] B. P. Abbott *et al.* (LIGO Scientific, Virgo, Fermi-GBM, INTE-GRAL Collaborations), Astrophys. J. **848**, L13 (2017).
[47] B. P. Abbott *et al.* (LIGO Scientific, Virgo Collaborations), Phys. Rev. Lett. **116**, 061102 (2016).
[48] B. P. Abbott *et al.* (LIGO Scientific, Virgo Collaborations), Phys. Rev. X **9**, 031040 (2019).
[49] R. Abbott *et al.* (LIGO Scientific, Virgo Collaborations), Phys. Rev. X **11**, 021053 (2021).
[50] T. T. Sun, Z. Y. Zheng, H. Chen, G. F. Burgio, and H.-J. Schulze, Phys. Rev. D **103**, 103003 (2021).
[51] A. Passamonti, M. Bruni, L. Gualtieri, A. Nagar, and C. F. Sopuerta, Phys. Rev. D **73**, 084010 (2006).
[52] A. Passamonti, N. Stergioulas, and A. Nagar, Phys. Rev. D **75**, 084038 (2007).
[53] C. Chirenti, M. C. Miller, T. Strohmayer, and J. Camp, Astrophys. J. Lett. **884**, L16 (2019).
[54] K. S. Thorne and A. Campolattaro, Astrophys. J. **149**, 591 (1967).
[55] R. Price and K. S. Thorne, Astrophys. J. **155**, 163 (1969).
[56] L. Lindblom and S. L. Detweiler, Astrophys. J. **53**, 73 (1983).
[57] S. L. Detweiler and L. Lindblom, Astrophys. J. **292**, 12 (1985).
[58] S. Chandrasekhar and V. Ferrari, Proc. R. Soc. A **432**, 247 (1991).
[59] G. F. Burgio, V. Ferrari, L. Gualtieri, and H.-J. Schulze, Phys. Rev. D **84**, 044017 (2011).
[60] C. V. Flores, Z. B. Hall II, and P. Jaikumar, Phys. Rev. C **96**, 065803 (2017).
[61] P. Jaikumar, A. Semposki, M. Prakash, and C. Constantinou, Phys. Rev. D **103**, 123009 (2021).
[62] Z. Bai, W.-j. Fu, and Y.-x. Liu, Astrophys. J. **922**, 266 (2021).
[63] C. Constantinou, S. Han, P. Jaikumar, and M. Prakash, Phys. Rev. D **104**, 123032 (2021).
[64] T. Zhao, C. Constantinou, P. Jaikumar, and M. Prakash, Phys. Rev. D **105**, 103025 (2022).
[65] T. Zhao and J. M. Lattimer, Phys. Rev. D **106**, 123002 (2022).
[66] A. Kunjipurayil, T. Zhao, B. Kumar, B. K. Agrawal, and M. Prakash, Phys. Rev. D **106**, 063005 (2022).
[67] A. Reisenegger and P. Goldreich, Astrophys. J. **395**, 240 (1992).
[68] D. Kumar, H. Mishra, and T. Malik, J. Cosmol. Astropart. Phys. 02 (2023) 015.
[69] Z. H. Li, U. Lombardo, H.-J. Schulze, and W. Zuo, Phys. Rev. C **77**, 034316 (2008).
[70] J.-B. Wei, J.-J. Lu, G. F. Burgio, Z.-H. Li, and H.-J. Schulze, Eur. Phys. J. A **56**, 63 (2020).
[71] N. K. Glendenning, Phys. Rev. D **46**, 1274 (1992).
[72] J. P. Jeukenne, A. Lejeune, and C. Mahaux, Phys. Rep. **25**, 83 (1976).
[73] M. Baldo, Int. Rev. Nucl. Phys. **8**, 1 (1999).
[74] R. B. Wiringa, V. G. J. Stoks, and R. Schiavilla, Phys. Rev. C **51**, 38 (1995).
[75] R. Machleidt, K. Holinde, and C. Elster, Phys. Rep. **149**, 1 (1987).
[76] R. Machleidt, Adv. Nucl. Phys. **19**, 189 (1989).
[77] P. Grangé, A. Lejeune, M. Martzolff, and J.-F. Mathiot, Phys. Rev. C **40**, 1040 (1989).
[78] W. Zuo, A. Lejeune, U. Lombardo, and J. F. Mathiot, Nucl. Phys. **A706**, 418 (2002).
[79] I. Bombaci and U. Lombardo, Phys. Rev. C **44**, 1892 (1991).
[80] I. Bombaci, T. T. S. Kuo, and U. Lombardo, Phys. Rep. **242**, 165 (1994).
[81] W. Zuo, Z. H. Li, A. Li, and G. C. Lu, Phys. Rev. C **69**, 064001 (2004).
[82] G. F. Burgio and H.-J. Schulze, Astron. Astrophys. **518**, A17 (2010).
[83] F. Li, J.-J. Lu, Z.-H. Li, C.-Y. Chen, G. F. Burgio, and H.-J. Schulze, Phys. Rev. C **103**, 024307 (2021).
[84] H. Shen, F. Ji, J. Hu, and K. Sumiyoshi, Astrophys. J. **891**, 148 (2020).
[85] M. Baldo, G. F. Burgio, M. Centelles, B. K. Sharma, and X. Viñas, Phys. At. Nucl. **77**, 1157 (2014).
[86] M. Fortin, C. Providência, A. R. Raduta, F. Gulminelli, J. L. Zdunik, P. Haensel, and M. Bejger, Phys. Rev. C **94**, 035804 (2016).
[87] C. Y. Tsang, M. B. Tsang, P. Danielewicz, F. J. Fattoyev, and W. G. Lynch, Phys. Lett. B **796**, 1 (2019).
[88] Z. H. Luo, J. B. Wei, G. Chen, H. Chen, and H.-J. Schulze, Mod. Phys. Lett. **34A**, 1950202 (2019).
[89] H. Chen, W. Yuan, L. Chang, Y. X. Liu, T. Klähn, and C. D. Roberts, Phys. Rev. D **78**, 116015 (2008).
[90] T. Klähn, C. D. Roberts, L. Chang, H. Chen, and Y. X. Liu, Phys. Rev. C **82**, 035801 (2010).
[91] J. B. Wei, H. Chen, G. F. Burgio, and H.-J. Schulze, Phys. Rev. D **96**, 043008 (2017).
[92] J. P. Pereira, C. V. Flores, and G. Lugones, Astrophys. J. **860**, 12 (2018).
[93] J. Oppenheimer and G. Volkoff, Phys. Rev. **55**, 374 (1939).
[94] R. C. Tolman, Phys. Rev. **55**, 364 (1939).
[95] T. G. Cowling, Mon. Not. R. Astron. Soc. **101**, 367 (1941).
[96] W. Xu and D. Lai, Phys. Rev. D **96**, 083005 (2017).
[97] G. Lugones and A. G. Grunfeld, Universe **7**, 493 (2021).
[98] M. C. Rodríguez, I. F. Ranea-Sandoval, M. Mariani, M. G. Orsaria, G. Malfatti, and O. M. Guilera, J. Cosmol. Astropart. Phys. 02 (2021) 009.

[99] I. F. Ranea-Sandoval, O. M. Guilera, M. Mariani, and G. Lugones, Phys. Rev. D **106**, 043025 (2022).
[100] P. N. McDermott, H. M. Van Horn, and J. F. Scholl, Astrophys. J. **268**, 837 (1983).
[101] D. D. Doneva, E. Gaertig, K. D. Kokkotas, and C. Krüger, Phys. Rev. D **88**, 044052 (2013).
[102] K. S. Thorne, Rev. Mod. Phys. **52**, 299 (1980).
[103] M. J. Szczepańczyk *et al.*, Phys. Rev. D **104**, 102002 (2021).
[104] L. S. Finn and C. R. Evans, Astrophys. J. **351**, 588 (1990).
[105] V. A. Dommes and M. E. Gusakov, Mon. Not. R. Astron. Soc. **455**, 2852 (2016).
[106] V. Tran, S. Ghosh, N. Lozano, D. Chatterjee, and P. Jaikumar, arXiv:2212.09875.
[107] E. M. Kantor and M. E. Gusakov, Mon. Not. R. Astron. Soc. **442**, L90 (2014).
[108] H. Yu and N. N. Weinberg, Mon. Not. R. Astron. Soc. **464**, 2622 (2017).
[109] P. B. Rau and I. Wasserman, Mon. Not. R. Astron. Soc. **481**, 4427 (2018).
[110] B. P. Abbott *et al.*, Phys. Rev. Lett. **121**, 161101 (2018).
[111] M. Ruiz, S. L. Shapiro, and A. Tsokaros, Phys. Rev. D **97**, 021501(R) (2018).
[112] S. Khadkikar, A. R. Raduta, M. Oertel, and A. Sedrakian, Phys. Rev. C **103**, 055811 (2021).
[113] A. Bauswein, S. Blacker, G. Lioutas, T. Soultanis, V. Vijayan, and N. Stergioulas, Phys. Rev. D **103**, 123004 (2021).
[114] A. Figura, F. Li, J.-J. Lu, G. F. Burgio, Z.-H. Li, and H.-J. Schulze, Phys. Rev. D **103**, 083012 (2021).
[115] T. Regimbau, M. Evans, N. Christensen, E. Katsavounidis, B. Sathyaprakash, and S. Vitale, Phys. Rev. Lett. **118**, 151105 (2017).
[116] K. D. Kokkotas, T. A. Apostolatos, and N. Andersson, Mon. Not. R. Astron. Soc. **320**, 307 (2001).
[117] N. Andersson, V. Ferrari, D. I. Jones, K. D. Kokkotas, B. Krishnan, J. S. Read, L. Rezzolla, and B. Zink, Gen. Relativ. Gravit. **43**, 409 (2011).
[118] B. P. Abbott *et al.* (LIGO Scientific Collaboration), Classical Quantum Gravity **34**, 044001 (2017).
[119] L. S. Finn, Mon. Not. R. Astron. Soc. **227**, 265 (1987).
[120] G. Miniutti, J. A. Pons, E. Berti, L. Gualtieri, and V. Ferrari, Mon. Not. R. Astron. Soc. **338**, 389 (2003).
[121] S. Y. Lau and K. Yagi, Phys. Rev. D **103**, 063015 (2021).